Tuning the rod diameter of ZnO nanorods on porous silicon by incorporating graphene

Wen-Chang Huang[a], Jo Lun Chiu[b], Xin Dai Lin[b], Yu Ching Lin[b], Shin Chieh Tsai[b], Wei Ming Su[b], Chen Yuan Weng[b], Chien Cheng Lu[b], Chia Feng Lin[c], Hsiang Chen[b],*

[a] Department of Electro-Optical Engineering, Kun Shan University, Taiwan, ROC
[b] Department of Applied Material and Optoelectronic Engineering, National Chi Nan University, Taiwan, ROC
[c] Department of Materials Science and Engineering, National Chung Hsing University, Taichung 402, Taiwan, ROC

ABSTRACT

In this research, graphene was incorporated into the ZnO nanorods (NRs) growth in two different ways to enlarge the rod diameter of ZnO NRs on porous silicon (PS) substrates. We etched the P-type Si (1 0 0) wafer to form the PS layer in solution with HF and C_2H_5OH and H_2O_2 for appropriate time. Then, ZnO NRs with and without incorporating graphene were grown with solgel/hydrothermal methods on top of the PS substrates, respectively. To characterize the graphene incorporated ZnO NRs on PS substrates, multiple material analyses including field-emission scanning electron microscopy, energy dispersive X-ray spectroscopy, X-ray diffraction, photoluminescence, IV curves were used to study the graphene-incorporated ZnO NRs. Results indicate that ZnO NRs with larger diameters could be viewed with graphene included into the ZnO NR growth in two different ways. Furthermore, higher defect concentrations could be observed for the graphene-contained NRs.

In addition, the ZnO/PS contact exhibited rectifying electrical behaviors without graphene addition but non-rectifying electrical behaviors with graphene incorporation.

Tuning ZnO NRs growth on PS substrates with graphene is promising for future ZnO NRs/Si-based device applications.

Introduction

Owing to a wide direct bandgap of 3.37 eV and a large exciton binding energy of 60 meV, ZnO-based nanocomposites have attracted growing attention within the decade [1,2]. Recently, ZnO nanorods (NRs) integrated with silicon substrates have been proposed as components of various semiconductor devices such as gas sensors [3], UV detectors [4], and solar cells [5]. However, because of large mismatches in the lattice constant and high stress between the interface, porous silicon (PS) has been used to replace traditional silicon substrates to develop Si-based electronic and optoelectronic devices [6,7]. Among these ZnO nanorod-based devices, physical characteristics and material properties of the ZnO NRs have been demonstrated as one of the key factors that influence the overall performance of the ZnO-based nanodevices [8,9]. Until now, diversified ZnO nanostructures on PS have exhibited various functions as shown in Table 1. Therefore, modulating the geometric shapes or the sizes of the ZnO nanostructures could change the material properties and possibly improve the ZnO-based device performance. Moreover, tuning the rod diameter of the ZnO NR

might adjust the roughness and the exposed area of the ZnO layer, which might vary the optical and electrical behaviors of the ZnO nanocomposite [10]. On the other hand, ZnO NR growth incorporating graphene related materials has been reported to control the ZnO morphologies [11,12]. However, incorporation of graphene in the fabrication process to shrink or enlarge the NRs has not been clearly reported yet. In this study, graphene has been added into the ZnO NR growth process to modulate the rod diameter of the ZnO NRs on PS substrates.

Experimental

ZnO NRs with various graphene incorporated methods were grown on PS substrates. First, the PS layer was formed via etching of P-type Si (1 0 0) wafer in solution with $HF:C_2H_5OH:H_2O_2 = 1:2:1$ for 2.5 min. Then, ZnO NRs with and without incorporating graphene were grown with solgel/hydrothermal methods on top of the PS substrates, respectively. The seed layer solution was prepared by dissolving zinc acetate dihydrate $((ZnAc)Zn(CH_3COO)_2·2H_2O)$ and spread on the PS

Table 1
The research topics and functions of ZnO various nanostructures on PS.

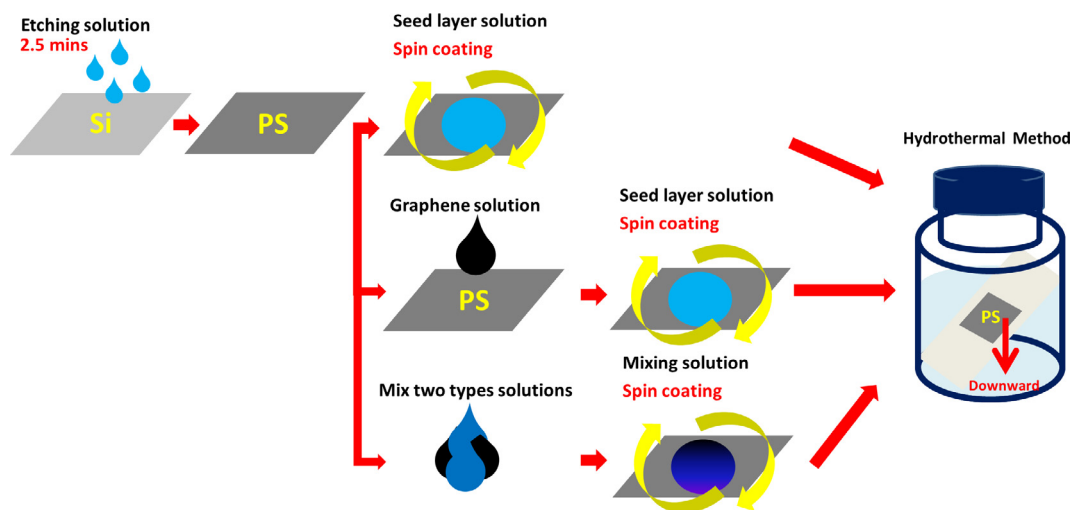|	Structures	Main research
This study	3 types ZnO NRs on PS substrates (add graphene or not)	The rod diameter of ZnO NRs by incorporating graphene
#1[13]	ZnO NWs grown on PS substrates	Orientation-enhanced growth and optical properties
#2[14]	ZnO nanocones/porous silicon heterostructures	White photoluminescence at room temperature
#3[15]	ZnO NWs grown on porous structure	Via a room-temperature routine for the fabrication of a 3D Si porous framework

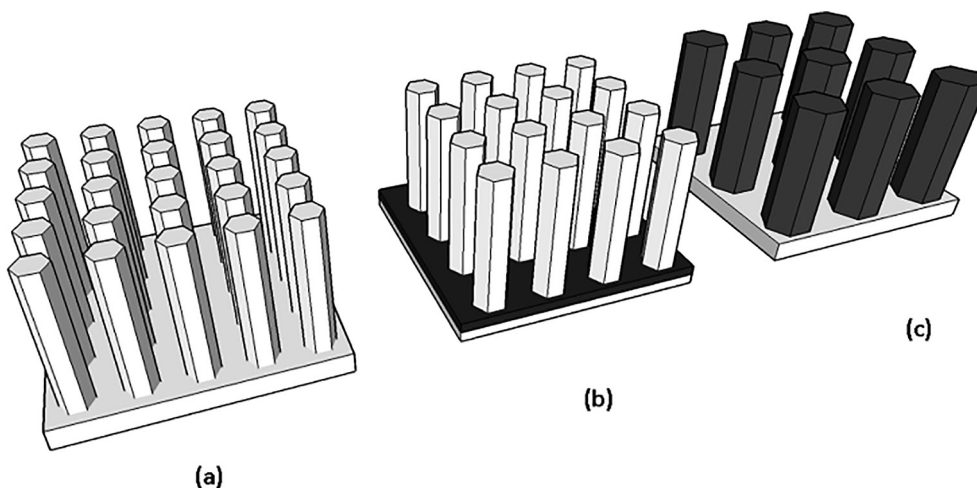

Fig. 1. Shows preparation of the samples.

Fig. 2. Illustrations of (a) ZnO NRs/PS (b) ZnO NRs/graphene/PS (c) Graphene-contained ZnO NRs/PS structures.

substrate, the seed layer was created by spreading the seed layer solution with baking. For the control group of sample, the ZnO seed layer was directly grown the PS substrate. Then, the ZnO NRs were hydrothermally grown in solution containing 0.05 M zinc nitrate (Zn(NO$_3$)$_2$·6H$_2$O) and 0.07 M Hexamethylenetetramine (HMT) at 85°c for 1 h [16]. The Fig. 1 shows the diagram for preparation of the samples. The growth of the first group is illustrated as Fig. 2(a). To incorporate graphene into the ZnO NRs fabrication process, we spread a layer of graphene by DV-100 (Ted Pella Inc.) pipettes on top of the PS substrate before depositing the seed layer. The graphene solution was synthesized by the Graphene company (Model S-ON10). After the graphene layer was baked and harden, the seed layer and the ZnO NRs were grown on the graphene/PS substrate with the same growth process. The growth of

the second group is illustrated as Fig. 2(b). The process of the fabrication process of the third group is as follows. The 5 ml same seed layer solution was added with graphene of 3 portions by DV-100 (Ted Pella Inc.) pipettes. After the seed layer solution was fully mixed with graphene, the graphene-contained seed layer was spread and grown on the PS substrate. Then, the NRs were hydrothermally grown in solution containing 0.05 M zinc nitrate (Zn(NO$_3$)$_2$·6H$_2$O) and 0.07 M Hexamethylenetetramine (HMT) at 85 °C for 1 h. The growth of the third group is illustrated as Fig. 2(c). To characterize the three distinct groups of the ZnO NRs with various graphene incorporation methods, multiple material analyses were used including FESEM, XRD, PL, and XPS. FESEM was used to investigate the size and the shape of the NRs and the XRD was used to examine the crystalline structures. Furthermore, PL was
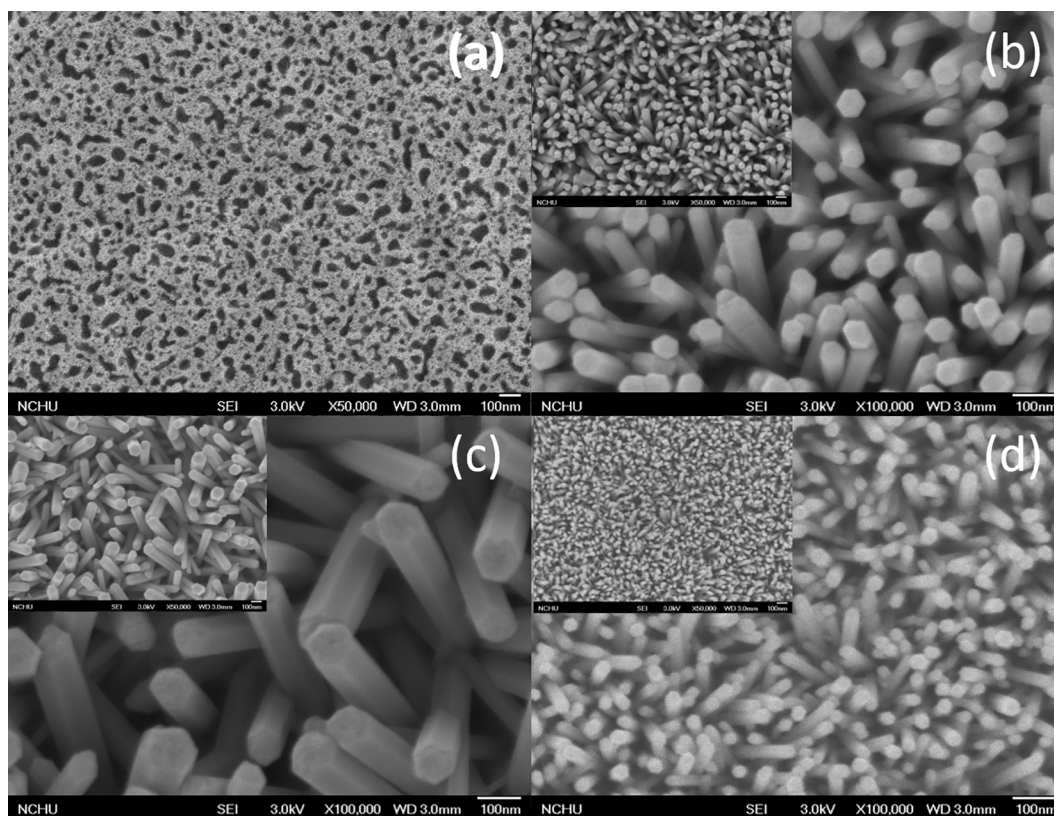
Fig. 3. FESEM images with 10,000 and 50,000 magnification rates of (a) PS substrate (b) ZnO NRs/PS (c) ZnO NRs/graphene/PS (d) graphene-contained ZnO NRs/PS structures.

used to investigate the optical properties and XPS was used to analyze the binding energies. I-V curves were used to analyze the rectifying effects.

Results and discussion

To view the surface morphologies of the PS substrate and the NRs, FESEM was used to study the size and the shape of the nanostructures. Fig. 3(a) shows the etched PS substrate with uniformly distributed nanopores with size around 100 nm. Moreover, Fig. 3(b)–(d) present the FESEM images of ZnO NRs/PS, ZnO NRs/graphene/PS, and graphene-contained ZnO NRs/PS structures, respectively. Fig. 3(b) shows that the diameter of the ZnO NRs of the normal ZnO NRs/PS structures was around 30–40 nm. As graphene was spread on top of the PS substrate, the rod diameters on the NRs/graphene/PS structure increased to 40–60 nm as shown in Fig. 3(c). Moreover, as graphene was included in the seed layer solution instead of being spread on the substrate, the rod diameter of the NRs of the graphene-contained ZnO NRs/PS structure was further increased to 80–100 nm. The rod size could be modulated by incorporating graphene in different ways as illustrated in Fig. 2(a)–(c). On the other hand, the NRs of the normal ZnO NRs/PS structure were more like perpendicularly grown from the substrate. In addition, the normally grown NRs were more densely distributed than the NRs incorporated graphene in two different ways. According to a single ZnO NR structure, eight planes are present. The top and bottom are polar planes with Zn^{2+} and O^{2-} terminated and the side non polar planes are without charged ions. Incorporating ingredients into the ZnO NR growth solutions might enhance or suppress the perpendicular

growth or the lateral growth. Spreading graphene before dripping the seed layer solution may suppress the reaction the Zn^{2+}-terminated top plane and cause the rod to become fatter. On the other hand, mixing graphene into the seed layer solution may enhance the reaction the Zn^{2+}-terminated top plane and cause the rod to become thinner [17,18].

Furthermore, EDX analyses of Fig. 4(a)–(c) shows that Zn, O, and Si are present on these three structures.

To further analyze these three structures, XRD was used to investigate the crystalline phases as shown in Fig. 5 [19]. Compared with the XRD pattern of the normal ZnO NRs/PS structure (JCPDS Card No. 36-1451), the intensity of the peak (0 0 2), which represents perpendicular growth, was similar. However, for the NRs/graphene/PS structure and graphene-contained ZnO NRs/PS structures, the peaks of crystalline phases in addition to (0 0 2) such as (1 0 0), (1 0 1), (1 0 2) and (1 1 0) were stronger than the control one. The result indicates that the ZnO NR growth incorporating graphene could not as perpendicular as the control one [20,21], consistent with the FESEM images as shown in Fig. 3. Moreover, graphene-contained ZnO NRs even had stronger (1 0 0), (1 0 1), (1 0 2) and (1 1 0) peak intensity than all the other structures.

Furthermore, the optical properties of these ZnO NRs were investigated by the PL measurements as shown in Fig. 6 [22]. It is observed that the PL peak around 375 nm in the spectrum represented the near band edge (NBE) emission, and the PL peak around 560 nm in the spectrum represented the defect luminescence, which might be attributed to oxygen vacancies in the ZnO NRs. It can be seen that the normal ZnO NRs/PS structure had much stronger NBE emission than the defect
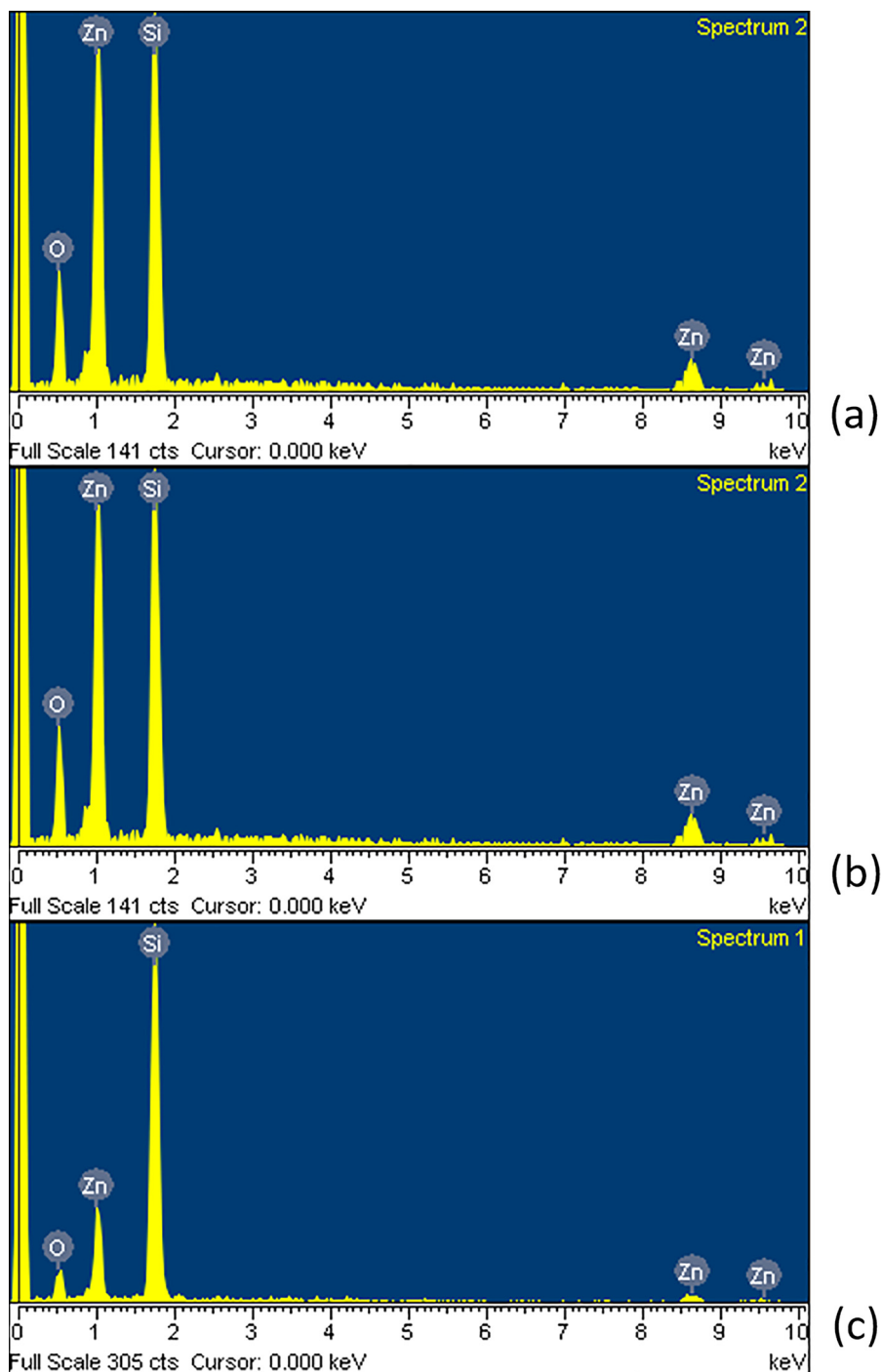
Fig. 4. EDX spectra of (a) ZnO NRs/PS (b) ZnO NRs/graphene/PS (c) Graphene-contained ZnO NRs/PS structures.

luminescence. However, for the for the NRs/graphene/PS structure and graphene-contained ZnO NRs/PS structures, the defect luminescence was stronger than the NBE emission as shown in Fig. 6. Since the graphene-incorporated NRs had compositions of various crystalline phases as indicated in the XRD patterns, more defect concentrations might be distributed in the ZnO NRs [23,24]. In addition, the graphene-contained ZnO NRs had the strongest defect luminescence, which was consistent with the XRD pattern of stronger (1 0 0), (1 0 1), (1 0 2) crystalline phases.

To further examine the presence of the defect, the O 1 s XPS measurement was used to study the oxygen binding energy. The O 1 s spectra of the ZnO NRs/PS [25], and ZnO NRs/graphene/PS and graphene-contained ZnO NRs/PS structures are shown in Fig. 7(a)–(c), respectively. These spectra were deconvoluted into two-peak profiles consisting of the peak energy of 530.5 eV and the peak energy of 532 eV. The O 1 s binding energy of 530.5 eV signifies Zn-O-Zn binding while the binding energy of 532 eV represents Zn-O-H binding related to the presence of the oxygen-vacancy defects in ZnO [26,27].
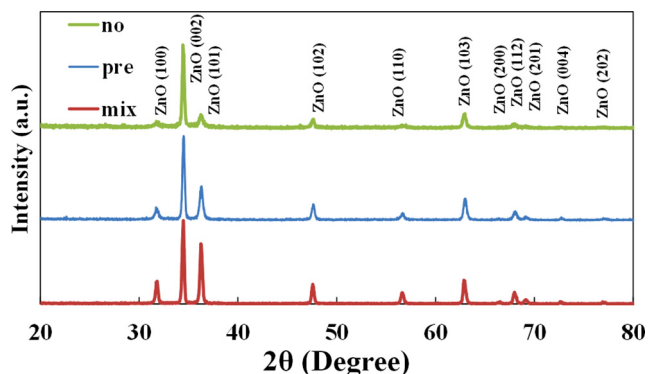
Fig. 5. XRD patterns of ZnO NRs/PS (no), ZnO NRs/graphene/PS (pre), and graphene-contained ZnO NRs/PS (mix) structures.
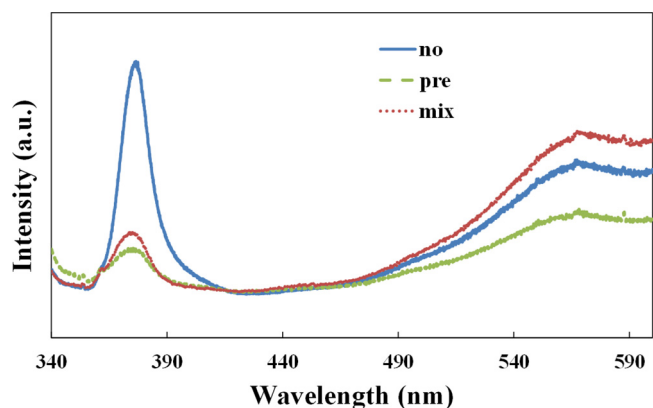

Fig. 6. PL measurements of ZnO NRs/PS (no), ZnO NRs/graphene/PS (pre), and graphene-contained ZnO NRs/PS (mix) structures.

Moreover, based on the calculation from the XPS spectra, Zn-O-Zn/Zn-O-H peak intensity ratio of the ZnO NRs/PS, and ZnO NRs/graphene/PS and graphene-contained ZnO NRs/PS structures were 3.83, 3.26, and 3.14 as shown in Fig. 7(a)–(c), respectively. Consistent with the PL measurements, the graphene-contained ZnO NRs/PS had the highest defect concentration. Similarly, the normal ZnO NRs/PS structure had the largest Zn-O-Zn/Zn-O-H peak intensity ratio and the largest NBE/defect luminescence peak intensity ratio at the same time.

Finally, we compared the I-V curves for the ZnO NRs/graphene/PS and graphene-contained ZnO NRs/PS structures as shown in Fig. 8(a) and (b). Since the ZnO NRs was n-type and the porous substrate and the p-type porous substrate was n-type, the rectifying effects could be clearly observed as shown in Fig. 8(a). As for the I-V curve for graphene-contained ZnO NRs/PS structures as shown in Fig. 8(b), no rectifying effect could be observed because plenty of oxygen-related defect with graphene containing might cause the ZnO NRs more neutral-like. Based on previous reports, the rectifying behaviors (Schottky contact) might be weakened by increasing the conductivity on porous silicon related contacts. Since incorporating graphene into ZnO nanorods could enhance the conductivity and weaken the rectifying effects. Therefore, the I-V curves became more non-rectifying (Ohmic contact like) [28–30].

Conclusions

In this study, ZnO NRs sogel/hydrothermal growth on PS substrates was modulated by incorporation of graphene in two different ways. Results indicate that larger diameter of ZnO NRs could be observed with graphene included into ZnO fabrication process. Furthermore, multiple material analyses indicate that higher defect concentrations in ZnO NRs could be observed by incorporating graphene. The graphene-modulated ZnO NR growth shows promises for future ZnO NR/Si nanostructure-based device applications.
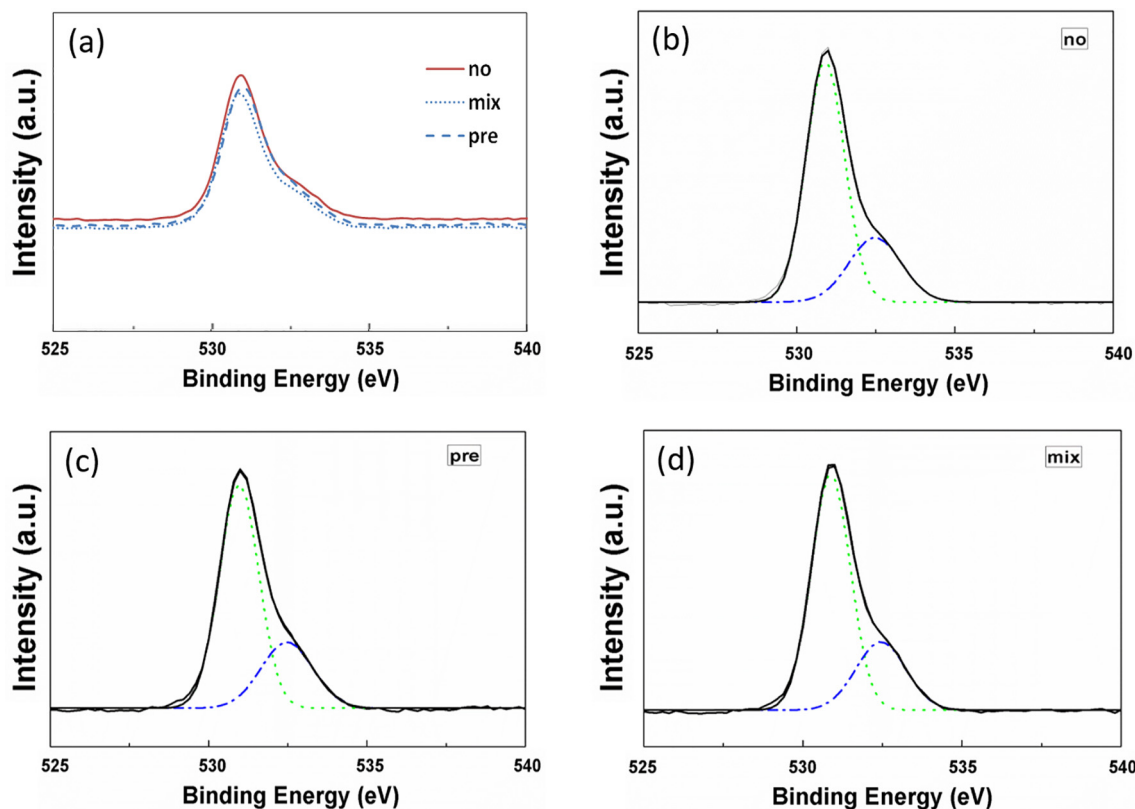

Fig. 7. The O1s XPS spectra of (a) ZnO NRs/PS, (b) ZnO NRs/graphene/PS, and (c) Graphene-contained ZnO NRs/PS structures.
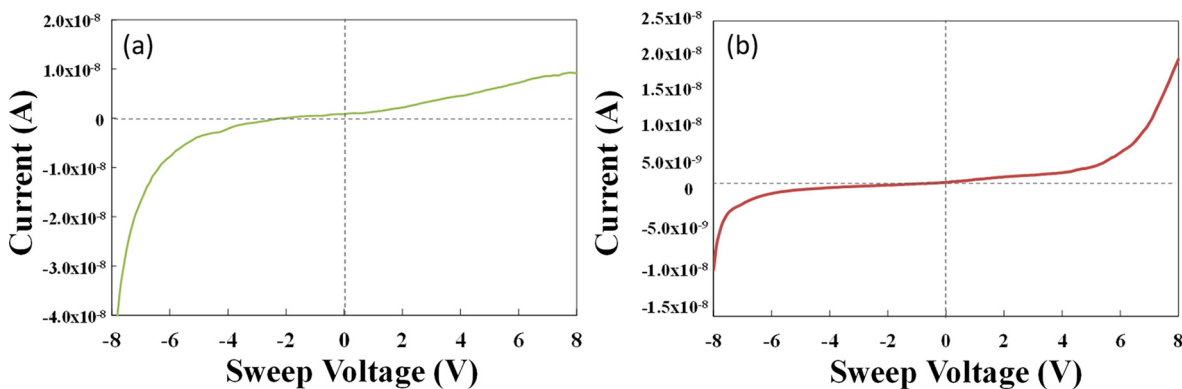
Fig. 8. I-V curves for (a) The ZnO NRs/graphene/PS and (b) Graphene-contained ZnO NRs/PS structures.

References

[1] Wang X, Summers CJ, Wang ZL. Large-scale hexagonal-patterned growth of aligned ZnO nanorods for nano-optoelectronics and nanosensor arrays. Nano Lett 2004;4(3):423–6.

[2] Huang S-C, et al. ZnO nanoflakes on silver wires with antibacterial effects. Ceram Int 2016;42(6):7848–51.

[3] Hassan JJ, et al. Room temperature hydrogen gas sensor based on ZnO nanorod arrays grown on a SiO$_2$/Si substrate via a microwave-assisted chemical solution method. J Alloy Compd 2013;546(5):107–11.

[4] Ma X, et al. Electrically pumped ZnO film ultraviolet random lasers on silicon substrate. Appl Phys Lett 2007;91:251109.

[5] Galoppini E, et al. Fast electron transport in metal organic vapor deposition grown dye-sensitized ZnO nanorod solar cells. J Phys Chem B 2006;110(33):16159–61.

[6] Salman KA, Omar K, Hassan Z. Improved performance of a crystalline silicon solar cell based on ZnO/PS anti-reflection coating layers. Superlattices Microstruct 2011;50(5):517–28.

[7] Thjeel HA, et al. Fabrication and characteristics of fast photo response ZnO/porous silicon UV photoconductive detector. Adv Mater Phys Chem 2011;1:70–7.

[8] Eswar K, et al. Hydrothermal growth of flower-like ZnO nanostructures on porous silicon substrate. J Mol Struct 2014;1074:140–3.

[9] Yan D, et al. Electrochemical deposition of ZnO nanostructures onto porous silicon and their enhanced gas sensing to NO$_2$ at room temperature. Electrochim Acta 2014;115:297–305.

[10] Chen H, et al. Characterizations of zinc oxide nanorods incorporating a graphene layer as antibacterial nanocomposites on silicon substrates. Ceram Int 2016;42(2):3424–8.

[11] Pruna A, et al. Seed-free electrodeposition of ZnO bi-pods on electrophoretically-reduced graphene oxide for optoelectronic applications. Ceram Int 2015;41(2):2381–8.

[12] Pruna A, et al. Enhanced electrochemical performance of ZnO nanorod core/poly-pyrrole shell arrays by graphene oxide. Electrochim Acta 2016;187:517–24.

[13] Hsu HC, et al. Orientation-enhanced growth and optical properties of ZnO nanowires grown on porous silicon substrates. Nanotechnology 2005;16(2):297.

[14] Marin O, et al. On the origin of white photoluminescence from ZnO nanocones/ porous silicon heterostructures at room temperature. Superlattices Microstruct 2015;79:29–37.

[15] Wang Z, Hou Z. Room-temperature fabrication of a three-dimensional porous silicon framework inspired by a polymer foaming process. Chem Commun 2017;53:8858.

[16] Steiger P, et al. Hydrothermally grown ZnO electrodes for improved organic photovoltaic devices. Thin Solid Films 2018;645:417–23.

[17] Chen H, et al. Tuning zinc oxide nanorods on SiO$_2$ substrates byincorporating graphene. Digest J Nanomater Biostruct 2018;13(2):375–80.

[18] Yu T-Y, et al. Fabrication and material analysis of zinc oxide nanorods grown on gallium nitride substrate. J New Mater Electrochem Syst 2016;19(4):181–240.

[19] Dobrucka R, Długaszewska J. Biosynthesis and antibacterial activity of ZnO nanoparticles using Trifolium pratense flower extract. Saudi J Biol Sci 2016;23(4):517–23.

[20] Zhang X, et al. Effect of aspect ratio and surface defects on the photocatalytic activity of ZnO nanorods. Sci Rep 2014;4:4596.

[21] Tian ZR, et al. Complex and oriented ZnO nanostructures. Nat Mater 2003;2:821–6.

[22] Musa I, Qamhieh N, Mahmoud ST. Synthesis and length dependent photoluminescence property of zinc oxide nanorods. Results Phys 2017;7:3552–6.

[23] Mclaren A, et al. Shape and size effects of ZnO nanocrystals on photocatalytic activity. J Am Chem Soc 2009;131(35):12540–1.

[24] Garcia SP, Semancik S. Controlling the morphology of zinc oxide nanorods crystallized from aqueous solutions: the effect of crystal growth modifiers on aspect ratio. Chem Mater 2007;19(16):4016–22.

[25] Wang H, et al. Facile fabrication of porous ZnS and ZnO films by coaxial electrospinning for highly efficient photodegradation of organic dyes. Photochem Photobiol 2018;94:17–26.

[26] Mal S, et al. Defect-mediated ferromagnetism and controlled switching characteristics in ZnO. J Mater Res 2011;26(10):1298–308.

[27] Shannon RD. Revised effective ionic radii and systematic studies of interatomic distances in halides and chalcogenides. Acta Crystallogr, Sect A: Cryst Phys Diffr Theor Gen Crystallogr 1976;32:751–67.

[28] Kanungo J, et al. The effect of different metal electrodes on the performance of ZnO/p-Si/Al hetero-structure for hydrogen detection. IEEE Sens J 2017;17:8290–6.

[29] Beale MIJ, et al. An experimental and theoretical study of the formation and microstructure of porous silicon. J Cryst Growth 1985;73:622–36.

[30] Pulsford NJ, et al. Behavior of a rectifying junction at the interface between porous silicon and its substrate. J Appl Phys 1994;75(1):636.